JOURNAL OF MATERIALS SCIENCE 32 (1997) 2155–2162

# Fracture chemistry of $\delta$-$Al_2O_3$ (Saffil) fibres in an MgLi matrix environment

S. KÚDELA, V. GERGELY
*Institute of Materials and Machine Mechanics, Slovak Academy of Sciences, 836 06 Bratislava, Slovakia*

S. BAUNACK, A. JOHN, S. OSWALD, K. WETZIG
*Institut für Festkörper- und Werkstofforschung Dresden e.V., Institut für Festkörperanalytik und Strukturforschung, Postfach 270016, D-01171 Dresden, Germany*

Fracture surfaces of $\delta$-$Al_2O_3$ (Saffil) fibres embedded in an Mg–8 wt% Li matrix by the pressure infiltration process were investigated by *in situ* Auger electron spectroscopy to study the chemistry of embrittlement of the former, resulting from a cross-section attack by the molten Mg–8 wt% Li matrix. The unaffected fibres failed transgranularly without any indications of silica being the crack-controlling flaws. Displacement reductive reactions between fibre constituents ($\delta$-$Al_2O_3$, silica) and penetrating lithium and magnesium species produce the phases that disturb the structural coherency of fibres and provide the paths for the crack propagation. In the early fibre/matrix reaction stage (slightly affected fibres) there are elemental silicon and aluminium and, most likely, also $Li_2O$ that cause the intergranular fracture of fibres, whereas in the advanced reaction stage (strongly affected fibres), MgO is predominantly formed and the fracture propagates throughout the fibres via the MgO-enriched regions.

## 1. Introduction

Ultralight magnesium-lithium alloys (1.3–1.6 g cm$^{-3}$) provide a promising basis for the development of structural metallic materials with a high strength-to-weight ratio. Commercially available MgLi alloys, such as LA 141 (USA) or MA 21 (USSR–Russia), are based on the primary Mg–Li system (up to $\sim$15 wt % Li) containing some additional elements (aluminium, zinc, cadmium, silver) to increase the strength and deformation characteristics. However, conventional strengthening mechanisms (precipitation hardening, work hardening) are of limited efficiency here, because of overageing effects and low activation energy for creep [1]. This deficiency is associated with exceedingly high vacancy concentration and mobility of lithium atoms, resulting in rapid coarsening of precipitates and promotion of dislocation climb. As a consequence, MgLi alloys exhibit pronounced creep even at room temperature so that, for example, LA 141 (Mg–14 wt % Li–1 wt % Al) cannot be applied as a carrying structural element operating at slightly elevated temperatures [2].

Composite approach seems to be the only way to overcome the above-mentioned intrinsic limitations concerning the deformation behaviour of the MgLi matrix. Advanced $\delta$-$Al_2O_3$ type ceramic fibres (Saffil, Saffil is a trademark of Imperial Chemical Industries) pretend to be a suitable reinforcement that will raise the bulk density of the final composite products only slightly. Such composite materials can be manufactured by pressure infiltration of fibrous preforms; however, the Saffil fibres (SFs) are susceptible to through-section attack by matrix elements during processing, which gives rise to the embrittlement of fibres, probably due to the grain-boundary penetration of lithium [3]. Even though a remarkable strengthening effect of SFs in an Mg12Li matrix has been reported [3] such embrittlement can significantly reduce the reinforcing efficiency of SFs, in particular concerning the creep resistance, because of the SFs breakage and increase of tertiary creep rate [4]. Thus, an understanding of chemical phenomena that affect the fracture of SFs embedded in an MgLi matrix is of major relevance for these composite materials.

Assuming that the fracture propagates in SFs just along chemically affected regions, the composition of the fractured surfaces of SFs has been investigated by Auger electron spectroscopy (AES) in the current study to elucidate the chemistry of fracture paths in SFs, after the latter had been affected by molten Mg–8 wt % Li matrix during the pressure-infiltration procedure. The AES measurements were conducted *in situ* in a scanning Auger microprobe because of its capability to detect lithium and the necessity of submicrometre lateral resolution (fibre diameter 2–5 μm), and under ultra-high vacuum (UHV) to expose the fibres without contamination. The AES investigation focused predominantly on the evaluation of energy shifts and changes in peak shapes of Auger transitions within the energy range 20–100 eV. This range

0022–2461  

involves the valence band transitions Li($KVV$), Mg($LVV$), Al($LVV$) and Si($LVV$) which are most sensitive to the anticipated chemical transformations that are the displacement reductive reactions between penetrating lithium and magnesium species, and SFs constituents ($Al_2O_3$, silica) yielding $Li_2O$ and MgO oxides [5]. Thus, the identification of $Li \rightarrow Li_2O$, $Mg \rightarrow MgO$, $Al_2O_3 \rightarrow Al$ and $SiO_2 \rightarrow Si$ chemical shifts should be possible.

## 2. Experimental procedure

### 2.1. Composite sample preparation

SFs/Mg8Li composite samples were prepared by pressure infiltration of SFs preform (30 mm × 5 nm × 5 mm), containing ≈ 20 vol % planar randomly oriented short Saffil fibres RF grade (ICI Runcorn, UK), with molten Mg–8 wt % Li alloy in the autoclave by complete submersion of the evacuated preform (10 Pa) into the molten metal (temperature, $T$) and subsequent application of an argon pressure (up to 6 MPa) within a time $t = t_2 - t_1$, which is defined as the interval between the onset of argon pressure inflow, $t_1$, and the moment the infiltrated preform is withdrawn from the liquid metal bath, $t_2$. The withdrawn sample was then cooled under argon pressure to room temperature. The infiltration procedure is described in detail elsewhere [5]. The Mg–8 wt % Li matrix alloy was prepared by casting of magnesium (purity 99.9%) and lithium (purity 99.95%) metals under an argon pressure.

### 2.2. Auger electron spectroscopy (AES)

The as-prepared SF/Mg8Li composite bars were V-notched and fractured in the AES apparatus (Perkin–Elmer PHI 660 SAM) under ultra-high vacuum (UHV) conditions ($5 \times 10^{-8}$ Pa). Auger electron spectra were taken at 10 keV electron energy and 10 nA current from central parts (point measurement) of the as-fractured fibre surface and from the same site after sputtering, respectively, attaining a lateral resolution of about 300 nm. The samples were sputtered with 4 keV $Ar^+$ ions in three cycles: (1) 0.9 min at 25 μA cm$^{-2}$, (2) + 1.5 min at 125 μA cm$^{-2}$, (3) + 7.6 min at 125 μA cm$^{-2}$, respectively. The spectra were recorded in the $EN(E)$ mode and treated by a five-point smoothing operation. The derivative spectra were obtained numerically.

### 2.3. Secondary ion mass spectrometry (SIMS)

Composite samples were selectively dissolved in a 10% bromine–methanol solution to extract SFs from the Mg8Li matrix. Extracted SFs were then impressed into an indium foil (purity 99.99%) and analysed by SIMS (IMMA, Applied Research Laboratory). The samples were sputtered with $Ar^+$ ions (18.5 keV at 40 μA) until all the fibres on the sputtered area (30 × 30 μm$^2$) were destroyed [6]. Both Li/Al and Mg/Al atomic ratios were determined semiquantitatively in SFs by registration of $^7Li^+$, $^{24}Mg^+$ and $^{27}Al^+$ secondary ions and normalizing the calculation using empirical sensitive factors. It should be noted that SIMS results can be significantly influenced by matrix effects [7].

## 3. Results

### 3.1. Preliminary AES experiments

Owing to the complexity of Auger electron emission, no fully successful model is available to interpret the changes of Auger spectra relating to the chemical shifts of individual elements. Hence, the identification of Auger lines is usually done by empirical comparison of unknown spectra to known standards ("finger print"). Because the precise identification of Auger spectra with respect to $Li \rightarrow Li_2O$ and $Mg \rightarrow MgO$ transformations is of great importance in our work and the reported data, especially as those for Li($KVV$) lines are controversional, we have established the corresponding Li($KVV$) and Mg($LVV$) lines from chemically well-defined substances as the standards in the series of preliminary AES experiments, which were conducted in the same way as described in Section 2.2. AE spectra for elemental magnesium were acquired from a UHV-broken magnesium bar (purity 99.99%) whereas the oxidic MgO state was arranged by subsequent oxyen-gas dosage up to 40 Langmuir (1 L = $1.33 \times 10^{-4}$ Pa s) on the freshly fractured magnesium bar surface. Spectra obtained are presented in Fig. 1a and b. To check the position of the Mg($LVV$) peaks

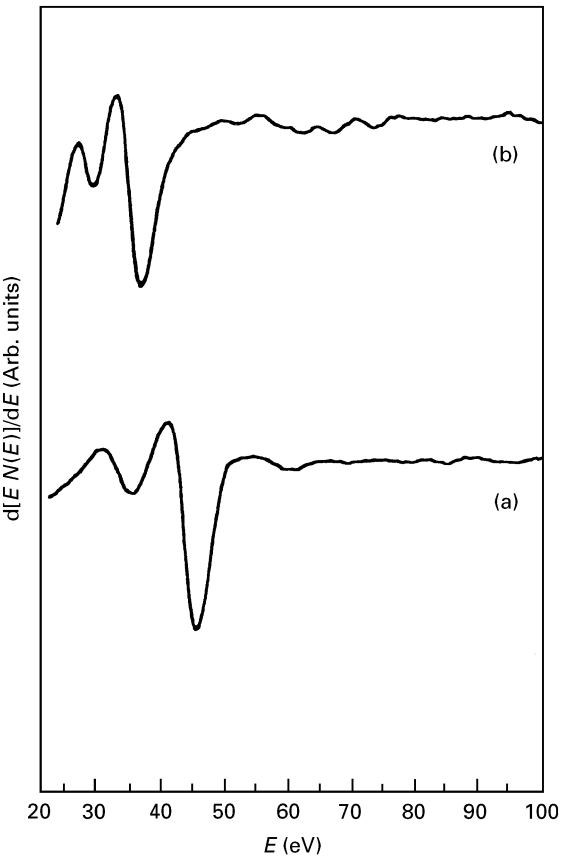


*Figure 1* Preliminary AES experiments performed with the magnesium standard: (a) Mg($LVV$) lines taken from as-fractured magnesium bars (elemental magnesium), (b) Mg( $LVV$) lines after oxygen-gas dosage (MgO).

for an MgO compound, an MgO powder standard (Aldrich Chemical Co., 99.99% purity) was used, after it had been covered with an AuPd film to preclude sample charging. The following principal Mg($LVV$) peaks were detected: 45 eV (elemental magnesium), 33 eV (MgO on the oxidized magnesium surface) and 32.5 eV (MgO standard). These data are close to those reported in the handbook [8].

A similar procedure was followed for the Li/$Li_2O$ system, where the external surface of soft lithium metal (99.9% purity) was scratched in UHV, to prepare a fresh oxygen-free surface for *in situ* AES measurement. By application of oxygen (up to 30 L), $Li_2O$ was fixed and the acquired AE spectra were then compared with that taken from AuPd-covered $Li_2O$ powder (Aldrich Chemical Co., unspecified purity). The results are shown in Fig. 2a and b, giving 50.5 eV for pure lithium, 39 eV for $Li_2O$ (oxidized lithium surfaces) and 41 eV ($Li_2O$ powder) as the strongest Li($KVV$) signals. These results agree well with the data reported by Hanke and Müller [9] for both pure lithium and $Li_2O$ (oxidized surface).

The reported Auger spectra belonging to the $Al_2O_3$/Al and $SiO_2$/Si chemical states are relatively well established, with the following prominent Al($LVV$) and Si($LVV$) peaks: 51 eV for $Al_2O_3$, 67 eV for aluminium, 78 eV for $SiO_2$ and 92 eV for silicon [8].

## 3.2. AES analysis of fractured fibres

### *3.2.1. AES analysis of unaffected SFs*

Attempts to gain AE spectra directly from virgin SFs have failed owing to the charging of analysed surfaces, so that SFs in an aluminium matrix environment were taken as an equivalent to those in the virgin state because they kept quite unaffected during infiltration with pure aluminium when only a thin surface silica film ($\sim$1 nm) undergoes the reaction with molten aluminium metal [10]. Characteristic AE spectra acquired *in situ* from as-fractured surfaces of SFs that have been infiltrated with molten aluminium ($T = 973$ K, $t = 120$ s) are presented in Fig. 3. In the rather simple shape of these spectra there are recognizable 35 and 53 eV peaks belonging, apparently, to $Al_2O_3$ (Fig. 3a). Note the weak 77 eV peak ($SiO_2$) has been observed only rarely (Fig. 3b). No significant Al($LVV$) peak at 67 eV belonging to elemental aluminium has been found, which provides the evidence that no electron-beam dissociation effects take place under the given conditions of AES analysis. However, the subsequent sputtering procedure has already led to the extensive evolution of the 67 eV Al($LVV$) line. As the similar Si($LVV$)-free AES lines have also been recorded from cross-sectional fibre cuts in metallographically treated SFs/Mg8Li composite samples, one can conclude that the silica is not essentially related to the fracture path propagation in unaffected SFs.

A typical morphology of the fractured surface of SFs in an aluminium matrix is shown in Fig. 4. The fracture appears to be homogeneous and it is difficult

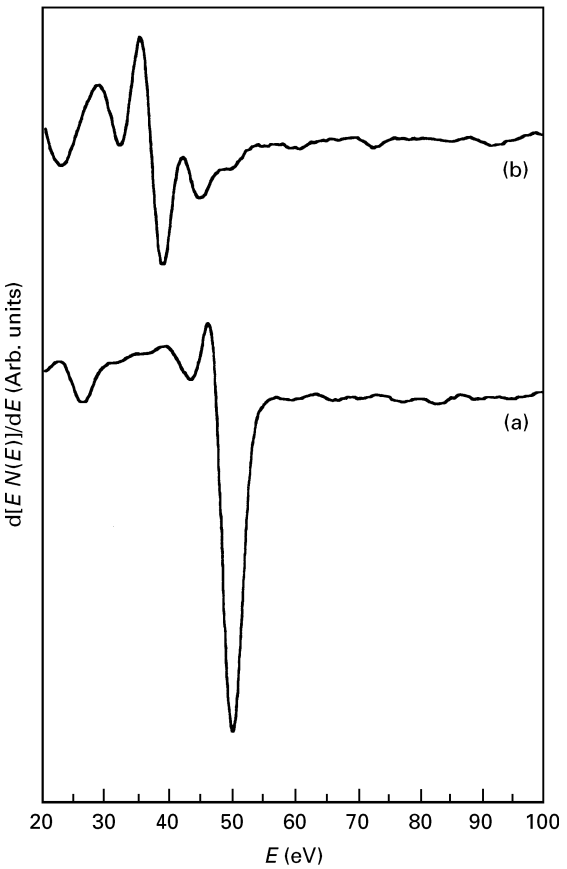


*Figure 2* Preliminary AES experiments performed with the lithium standard: (a) Li($KVV$) lines acquired from scratched lithium surface (elemental lithium), (b) Li($KVV$) lines after oxygen-gas application ($Li_2O$).

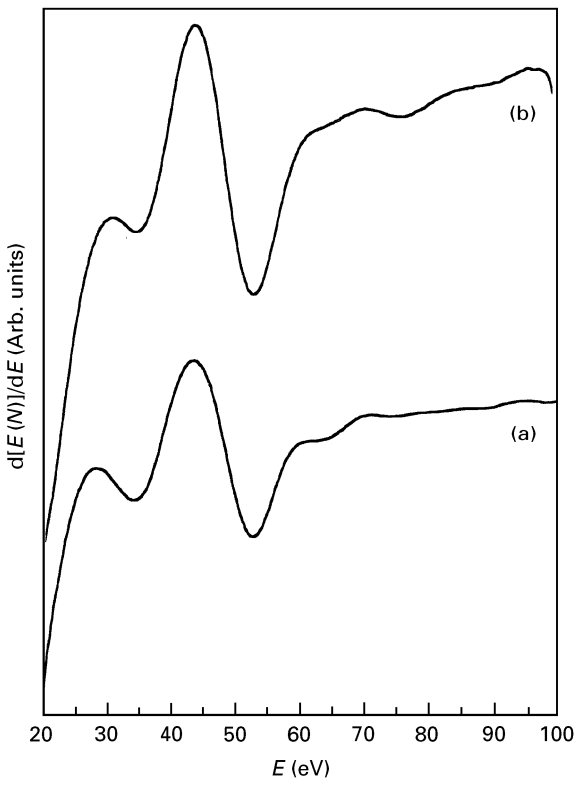


*Figure 3* AE spectra obtained from the fracture surface of unaffected SFs (embedded in an aluminium matrix): (a) characteristic AE lines with Al($LVV$) peaks at 36 and 53 eV ($Al_2O_3$), (b) AE lines exhibiting a weak 77 eV peak ($SiO_2$).

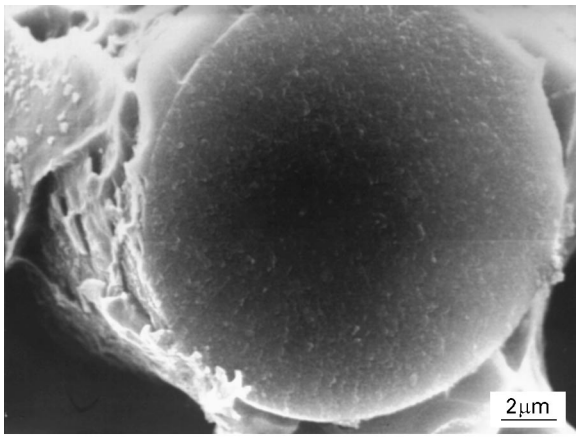


*Figure 4* Scanning electron micrograph of the fracture of unaffected SFs (aluminium matrix).

to detect the initiation point of the failure. Very fine facets are visible on the rather smooth cross-section of the fracture with a size of $\sim 50$ nm, which may correspond to the reported $\delta$-$Al_2O_3$ crystallite size [11]. However, the morphological details of facets are not perceptible.

### 3.2.2. AES analysis of slightly affected SFs

The chemistry of fracture paths in SFs that have reached the early stage of interaction with Mg8Li matrix are manifested by AES *in situ* results obtained from SFs/Mg8Li composites ($T = 898$ K, $t = 4$ s) exhibiting atomic ratios of Li/Al = 0.06 and Mg/Al = 0.007 (determined by SIMS analysis).

Fig. 5 shows typical AE spectra acquired from the as-fractured SF surface and those after sputtering. In comparison with unaffected SFs, these spectra are more complex, exhibiting two important features: (i) elemental aluminium Al($LVV$) (67 eV) was identified on the as-fractured fibre cross-section, and (ii) a strong Si($LVV$) signal was detected at 92 eV (elemental silicon) which tends to decrease markedly after sputtering. Note that in the same sample on the metallographically treated and unsputtered cross-sectional cut, elemental aluminium (67 eV) was found but no Si($LVV$) appeared. Thus, fracture paths in short-term infiltrated SFs closely correlate with the silicon-enriched regions. These, however, look rather thin and suggest a fall in Si($LVV$) intensity even after a short sputtering.

Both elemental silicon and aluminium are considered to be the by-products of displacement reductive reactions giving $Li_2O$ and MgO oxides. However, neither $Li_2O$ nor MgO were found explicitly on the fractured surfaces. Li($KVV$) peaks that should appear at 39 eV ($Li_2O$) can be overlaid with Al($LVV$) belonging to $Al_2O_3$ peaks situated, here, at 39.5 eV. This frustrates the parallel Li($KVV$) and Al($LVV$) detection. This assumption is supported by peak-to-peak comparison of Al($LVV$) line intensities: 39–55 eV in Fig. 5 with 36–53 eV in Fig. 3, which reveals that the 39 eV signal is far stronger than it should be, and it can be considered to be the overlapping of both

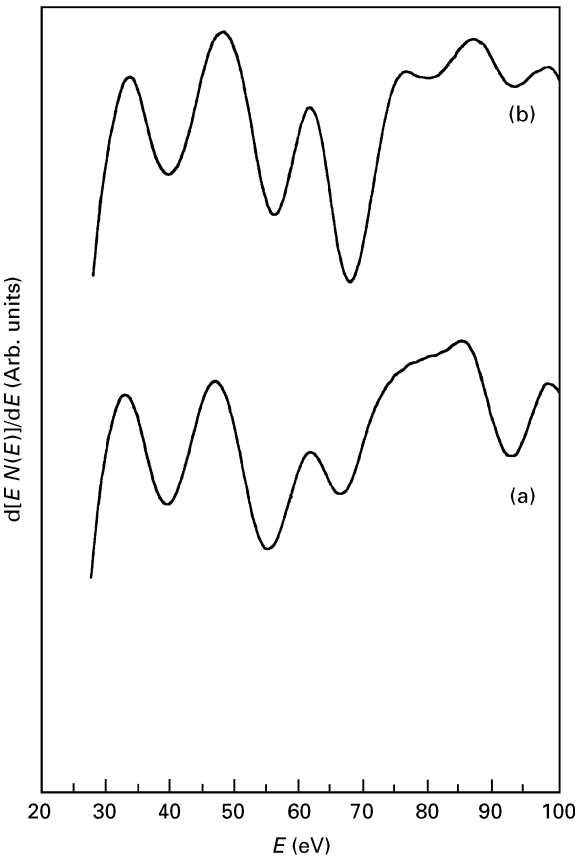


*Figure 5* AE spectra belonging to the slightly affected SFs (infiltration has been performed with Mg8Li alloy at $T = 898$ K, $t = 4$ s): (a) AE lines taken from as-fractured surface exhibiting Al($LVV$) peaks at 39.5 and 55 eV ($Al_2O_3$) and 67 eV (elemental aluminium) together with the Si($LVV$) peak at 92 eV (elemental silicon), (b) AE spectra taken from the same site after the sputtering procedure.

Al($LVV$) and Li($KVV$) lines. As seen, the aluminium oxide peaks in our experiments are slightly shifted towards higher energies in relation to the reported values [8], possibly due to the less-pronounced charging effect in SFs in the surrounding conductive matrix.

On the other hand, Mg($LVV$) peaks (33 and 44 eV) are definitely missing on the analysed SFs fracture surfaces, which suggests that magnesium does not participate in the damage of SFs in the early interaction stage.

Even if the above AE spectra are characteristic of the fracture of slightly affected SFs, there are also regions displaying AE spectra identical to those in Fig. 3. These unaffected regions are distributed randomly within the whole cross-fracture, which indicates the non-uniform fibre attack upon infiltration.

A scanning electron micrograph of slightly affected SFs is shown in Fig. 6. The fracture surface appears to be homogeneous throughout the whole cross-section, without any morphologically discernible reaction layer on the peripheral parts of fibres. In contrast to the unaffected SFs the fracture surface is more granular, though the size of the fracture facets remains unchanged. In several cases the point of failure initiation is recognizable in the internal parts of the fibre cross-section, as a rule.

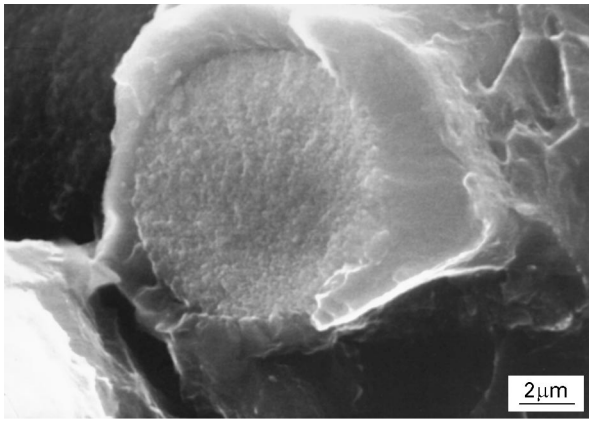


*Figure 6* SEM fracture of the slightly affected SFs.

### 3.2.3. AES analysis of strongly affected SFs

The SFs/Mg8Li composite sample that has been infiltrated for prolonged infiltration times ($T = 918$ K, $t = 420$ s) represents an advanced stage of SFs affection, displaying atomic ratios of Li/Al = 0.28 and Mg/Al = 0.06 (detected by SIMS).

A strong Mg($LVV$) signal belonging to MgO, wherein MgO (32 eV) appears either alone or parallel to $Al_2O_3$ (39 eV and 54 eV) is the major feature of the AE spectra acquired from the SFs fracture surface of the 918 K/420 s composite sample (Fig. 7). During sputtering the MgO peak remained unchanged, while the alumina peaks became either more intensive or disappeared completely, being replaced with that at 44 eV belonging to the elemental magnesium. This suggests that magnesia enriched regions are adjacent either to the $Al_2O_3$ grains or the metallic magnesium localities. Elemental magnesium has also frequently been found on the as-fractured fibre surfaces. The comparison of AE spectra taken from such "metallic" regions in SFs with that taken from Mg8Li matrix fracture regions in the same composite sample has revealed quite identical courses, where in parallel with the strong 44 eV signal (elemental magnesium), elemental aluminium (67 eV) is also significant (Fig. 8). Thus, the fracture of strongly affected SFs propagates predominantly along MgO localities when the large presence of "metallic" magnesium indicates the invasive percolation of the MgLi matrix alloy into the bulk of the fibres, and subsequent MgO formation by displacement reactions which are coupled with the production of elemental aluminium. An important observation is that no significant $Li_2O$ peaks were found in the considered AE spectra, even in the absence of the $Al_2O_3$ peak which may overlap the Li($KVV$) signal at 40 eV.

An extensive fibre–matrix reaction is observable on the fracture micrograph obtained from the SF locality (Fig. 9). The Mg–Al eutectic lamellae in Mg8Li matrix fracture that adhere radially to the fibre body, are visible, which suggests that alumina fibres are decomposed by the displacement reaction to such a degree that dissolved aluminium attains the eutectic concentration in the Mg8Li matrix. The decomposition of fibres proceeds apparently in the bulk, accompanied by considerable morphological changes of the fracture, and characterized by a complex structure with coarse grains (facets) having size of 150–200 nm, without any indication of the peripheral reaction layer forming. At the same time, however, the mean size of crystallites in corresponding SFs exhibit no changes compared to those in unaffected SFs (about 50 nm) as observed by transmission electron microscopy [12].

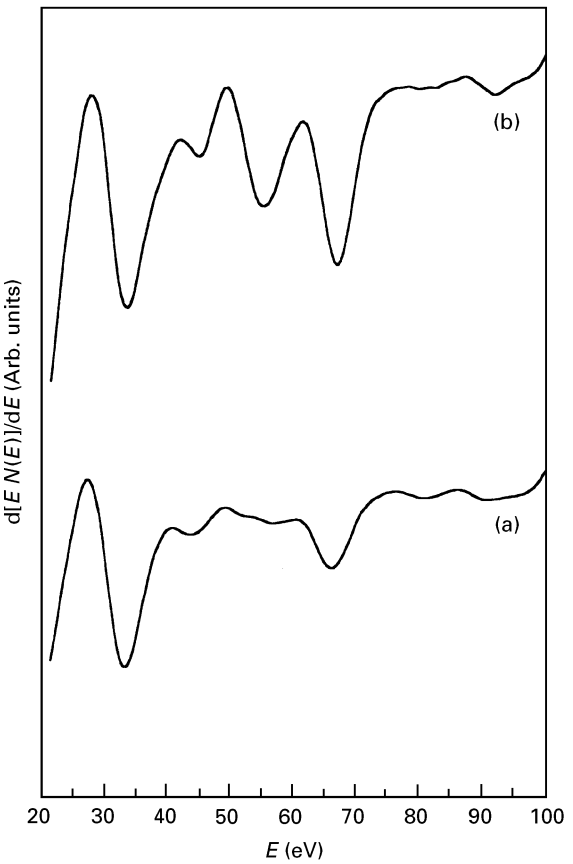


*Figure 7* AE spectra belonging to the strongly affected SFs (infiltration performed with Mg8Li alloy at $T = 918$ K, $t = 420$ s): (a) as-fractured surface with a strong Mg($LVV$) peak at 32.5 eV (MgO) and an Al($LVV$) peak at 67 eV (elemental aluminium), (b) the same site after sputtering, with Al($LVV$) peaks at 54 eV ($Al_2O_3$) and 67 eV (elemental aluminium) together with the remaining Mg($LVV$) peak at 32.5 eV (elemental magnesium).

### 3.2.4. Intermediately affected SFs

The infiltration of SFs with MgLi alloys is usually carried out at temperatures $T = 900$–$920$ K and time $t = 10$–$30$ s. AE spectra acquired from fractured surfaces of such "intermediately" affected SFs combine the features of both slightly and strongly affected SFs presented above, but being more like the latter, when Mg($LVV$) lines belonging to MgO and elemental magnesium are present. Nevertheless, Al($LVV$) peaks 54 eV ($Al_2O_3$) and 67 eV (elemental aluminium) remain dominant and the Si($LVV$) peak at 92 eV (elemental silicon) appears only exceptionally. Fracture morphology of intermediately affected SFs is comparable to that of slightly affected SFs.

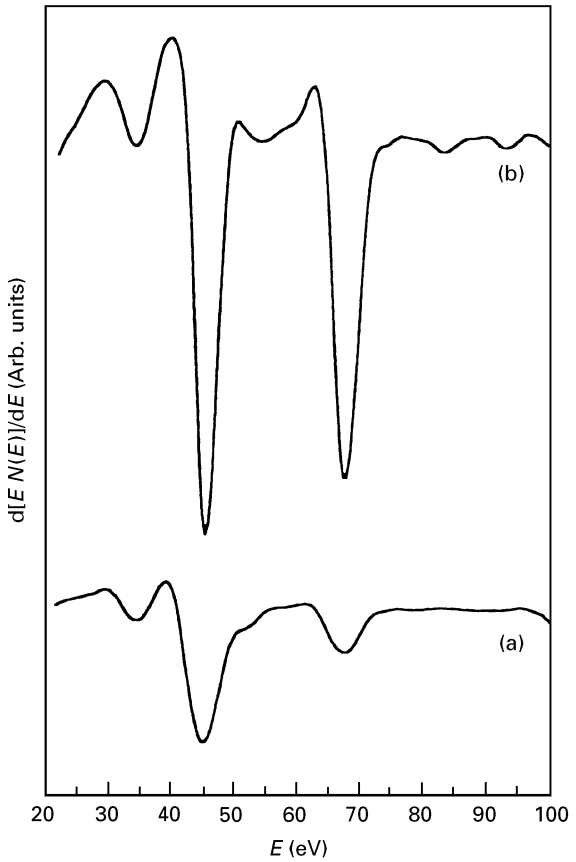


*Figure 8* (a) AE spectra taken from another site of the fracture surface of strongly affected SFs after sputtering, with the Mg($LVV$) peak 44 eV (elemental magnesium) and the Al($LVV$) line at 67 eV (elemental aluminium), (b) AE spectra acquired from MgLi matrix in the composite sample with strongly affected SFs (after sputtering).

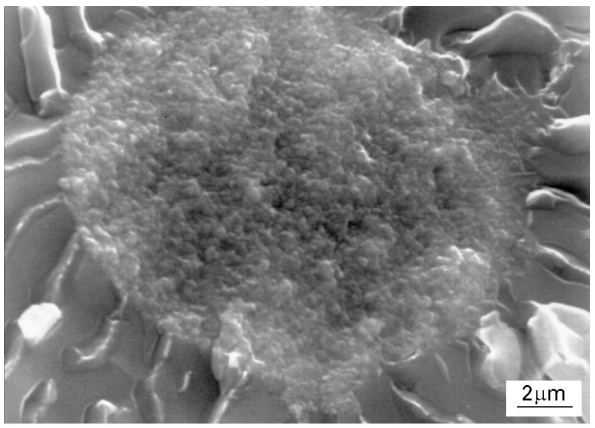


*Figure 9* Scanning electron micrograph of strongly affected SFs in the Mg8Li matrix with AlMg eutectic lamellae.

## 4. Discussion

Polycrystalline Saffil fibres RF grade consist of δ-$Al_2O_3$ crystallites (50 nm in size) as a major component and a small amount of silica (3–4 wt %) which stabilizes δ-polymorphism against the $\delta \rightarrow \alpha$ transformation and inhibits the crystallite growth during the thermal treatment. This results in a considerable Hall–Petch strengthening of the fibres. Silica is reported to be distributed throughout the δ-$Al_2O_3$ crystallites, being slightly concentrated at the grain boundaries [10]. Further details concerning the silica incorporation into SFs structure are not available.

Gel-solution spinning and subsequent firing ($\geqslant 1300$ K) as the manufacturing technology of SFs provide the feasibility for silica incorporation into transitive aluminas (including δ-$Al_2O_3$) to form a spinel-like $Al_2O_3$–$SiO_2$ solid solution by the solid-state reaction between alumina and silica xerogels during SFs manufacturing [13, 14]. The enrichment of δ-$Al_2O_3$ grain boundaries by silica (in the solid solution) can be attributed to the diffusion gradient of $Si^{4+}$ ions generated within solid-state reactions and, possibly, to the occurrence of residual nano-$SiO_2$ particles on alumina grains.

The current AES study of cross-fractured areas of SFs embedded in the aluminium matrix (unaffected state) has revealed that the fracture paths do not propagate via the silica-enriched region, e.g. the silica domains in SFs do not act as the fracture-controlling flaws. Considering that just grain boundaries in SFs are enriched by silica, one can conclude that the transcrystalline fracture mode seems to be characteristic of the failure of unaffected SFs. Such a fracture behaviour is consistent with the idea that silica is dissolved in the host alumina spinel lattice and SFs can be considered a nearly homogeneous material with silica inhomogeneities being, at most, of subcritical nano-size-scale in terms of crack expansion.

The polycrystalline nature of SFs gives rise to the cross-section attack during contact with molten MgLi alloys as a consequence of accelerated penetration of lithium and magnesium species along the grain boundaries of the fibres. In previous papers [5, 6] we have concluded that both lithium and magnesium penetrate the bulk SFs upon infiltration with molten Mg8Li alloy, resulting in a rapid incorporation of $Li^+$ ions into tetragonal δ-$Al_2O_3$ lattice, as indicated by the removal of the tetragonal distortion of the spinel units ($c/3a \rightarrow 1$) and also the appearance of enhanced disorder of the cation sites occupation. Although we have supposed the incorporation of $Mg^{2+}$ in the alumina spinel lattice upon infiltration [5], further experiments do not confirm this assumption [6].

According to the proposed reaction scheme, the grain boundaries in δ-$Al_2O_3$ (enriched by silica) serve as short-circuit diffusion paths for lithium and magnesium atoms that enter the displacement reactions

$$Al^{3+} + 3Li^0 = 3Li^+ + Al^0 \quad (1)$$

$$Si^{4+} + 4Li^0 = 4Li^+ + Si^0 \quad (2)$$

$$2Al^{3+} + 3Mg^0 = 3Mg^{2+} + 2Al^0 \quad (3)$$

$$Si^{4+} + 2Mg^0 = 2Mg^{2+} + Si^0 \quad (4)$$

yielding the $Li_2O$ and MgO oxides and elemental $Si^0$ and $Al^0$ by-products. Under the given reaction conditions, these reactions are thermodynamically favourable [15]. $Li^+$ ions that are generated by Reactions 1 and 2 will be incorporated into the spinel lattice of δ-$Al_2O_3$ to form the sequence of metastable mixed spinels.

The presented AES analysis results suggest that just the displacement Reactions 1–4 are responsible for the damage of SFs, as clearly manifested by the explicit detection of almost the complete series of anticipated reaction products ($Si^0$, $Al^0$, MgO) on the *in situ* analysed fibre fractures.

Reactions 1 and 2 seem to dominate in the early stage of SFs attack which provides the only plausible explanation of $Al^0$ and $Si^0$ appearance without any parallel Mg($LVV$) detection on the analysed surfaces. The strong Si($LVV$) signal provides evidence that the Auger analysis has, indeed, been made on grain-boundary surfaces, e.g. the intergranular fracture mode is characteristic of the slightly affected SFs. There are indications that $Li_2O$, as an intermediate product in the above-depicted reaction scheme, is also present on the fracture surface of slightly affected SFs. Hence, the topotactic $Li^+$ incorporation into $\delta$-$Al_2O_3$ lattice is impeded compared to lithium grain-boundary diffusion and then the $Li_2O$ formation. Even though the incorporation of $Li^+$ ions proceeds in the framework of the sublattice of oxygen anions, which provides a kinetically favourable route, there are at least two restricting factors: (i) cation vacant sites in the defective $\delta$-$Al_2O_3$ lattice are gradually eliminated by the ion-exchange reaction, (ii) the upper concentration limit of $Li^+$ dissolution is determined by the stoichiometric $LiAl_5O_8$ composition (2.6 wt % Li). Thus, the intergranular $Li_2O$ would not fully disappear.

Reactions 3 and 4 become more significant further into the reaction course, because the strongly affected SFs fail prevailingly along the MgO phase-enriched regions. Divalent $Mg^{2+}$ ions, like $Li^+$, can also enter the alumina spinels to stabilize them, as reported in the context of the $\delta$-$Al_2O_3$ structure study [16]. Because the available cation vacancies are preferentially eliminated by $Li^+$ ions, the next $Mg^{2+}$ incorporation cannot be accomplished. Moreover, the efficiency of the cation site occupation in transitive aluminas by $Mg^{2+}$ ions, is substantially lower than those by $Li^+$ [17]. As a result, MgO should be a stable phase and does not enter the next solid-state reactions upon infiltration.

As seen above, in the early stage of infiltration, only lithium participates in the cross-section attack of fibres, and magnesium penetration into fibres is retarded. When the infiltration is carried out with pure magnesium, the MgO formation in bulk of SFs does not occur. These observations clearly demonstrate that the penetration of magnesium into SFs upon infiltration with molten MgLi alloys is promoted by lithium. The possible explanation lies in the conception of Hallstedt *et al.* [18] who have explained the extensive formation of MgO in bulk SFs during prolonged thermal treatment of SFs/Mg composites above the eutectic temperature of the Al–Mg system (710 K), by the creation of low-melting eutectic AlMg intergranular liquid that facilitates the penetration of magnesium into the fibre bulk. Similarly, we can assume that the appearance of low-melting liquid Al–Si and/or Al–Si–Li intergranular domains results from rapid lithium grain-boundary diffusion and subsequent formation of elemental aluminum and silicon by Reactions 1 and 2. The aluminium-rich corner of the ternary Al–Si–Li diagram is shown in Fig. 10 where the Al–D line involving the point $n = 908$ K separates two eutectic systems: $E_1$ ($838 \pm 3$ K; 88.45 wt % Al, 11.5 wt % Si, 0.05 wt % Li) and $E_2$ ($868 \pm 2$ K; 88.8 wt % Al, 2 wt % Si, 9.2 wt % Li) [19]. The binary Al–Si system behaves in essentially the same manner as $E_1$. Hence, the metallic liquid can be formed in the grain-boundary regions of SFs under the given infiltration conditions which allow the percolation of molten MgLi matrix into individual SFs and the subsequent bulk formation of MgO only, because $Li_2O$ formation is thermodynamically less favourable [15]. This idea is also supported by the extensive alloying of MgLi matrix with aluminium and subsequent eutectic lamella formation that has been observed by SEM and detected by EDX in SFs/Mg8Li composites. In contrast, SFs/Mg exhibits only negligible aluminium concentration in the magnesium matrix. As believed, metallic aluminium produced by displacement reductive reactions drains from the SFs bulk into the MgLi matrix along the constituted liquid metal pathways.

Consequently, new phases that are formed by Reactions 1–4 act as flaws disturbing the structural coherency of SFs, thus providing the paths for crack propagation. In context with the previous discussion, two dominant types of flaw can be considered to affect the fracture of SFs in the MgLi matrix: (i) intergranular $Li_2O$ together with Al–Si and/or Al–Si–Li metallic domains (slightly affected SFs), (ii) MgO regions appearing frequently together with metallic magnesium and aluminium (strongly and intermediately affected SFs).

Because there are no distinguishable local details of fracture facets in the scanning electron micrographs of the fibre surfaces, in particular in terms of the metallic components distribution, it is difficult to make any assumption concerning the possible failure

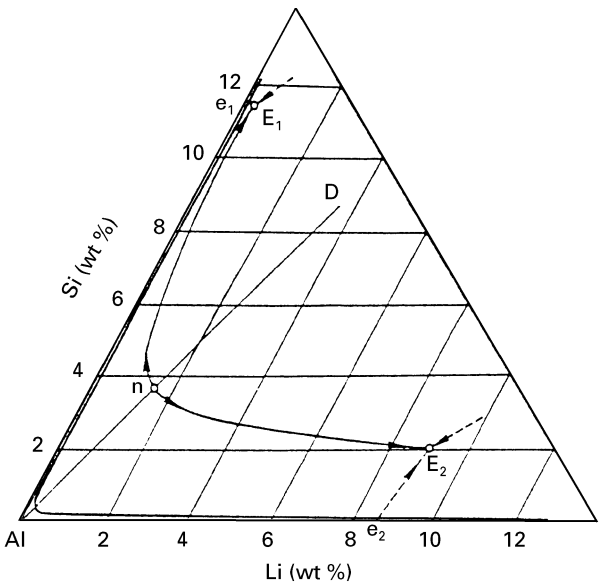


*Figure 10* The section of the aluminium-rich corner of the ternary Al–Si–Li diagram [19].

mechanism of the fibres. It appears that the reaction products can be considered to be the interphases at grain boundaries of SFs that include both brittle oxides ($Li_2O$, MgO) and ductile metals (aluminium, Al–Si, magnesium, etc.). It follows from the analysis of Evans *et al.* [20], that despite the complexity of this problem, the fracture energy of interphases often coincides with the fracture energy of the interphase material itself and the fracture path selection is governed by the appearance of the more brittle constituent. Thus, at this point, MgO and, to a lesser degree, $Li_2O$ seem be the major reason for the SFs embrittlement due to molten MgLi alloy attack.

## 5. Conclusion

An investigation by *in situ* Auger electron spectroscopy has been made of the chemistry of fracture paths of SFs which had been affected by a molten Mg8Li matrix during infiltration. Unaffected SFs (represented by that embedded in an aluminium matrix) have exhibited prevailingly transgranular fracture, without no evidence of silica acting as the crack-controlling flaw. During contact of SFs with molten Mg8Li matrix, both magnesium and lithium species penetrate into the bulk of the fibres, entering the displacement reductive reactions with the fibre components (alumina, silica). The products are considered to be the flaws that govern the fracture behaviour of fibres. In the early stage of interaction, lithium seems to be the only agent that penetrates into the fibre bulk along the grain boundaries, forming $Li_2O$ and elemental silicon and aluminium which act as the intergranular flaws upon fibre fracture. On the other hand, during further reaction, the percolation of magnesium into the fibre bulk occurs, and the failure of the considered fibres propagates predominantly along MgO-enriched regions.

## Acknowledgements

This work was supported by Sächsisches Staatsministerium für Wissenschaft und Kunst under project number 7541.83-IFW/404, and the Grant Agency for Science of the Slovak Republic (Project 2/74/93).

## References

1. E. HORNBOGEN and K. SCHEMME, in "Proceedings of the 47th Annual World Magnesium Conference" Cannes (France), May 1990 (ed. by International Magnesium Association, 1990) p. 67.
2. M. E. DRITS, F. M. YELKHIN, I. I. GURYEV, B. I. BONCHAREV, V. F. TROKHOVA, A. D. SERGHYEVSKAYA and T. N. OSOKHINA, "Magnesium – Lithium Alloys" (Metallurgia, Moscow, 1980) in Russian.
3. J. F. MASON, C. M. WARWICK, P. J. SMITH, J. A. CHARLES and T. W. CLYNE, *J. Mater. Sci.* **24** (1989) 3934.
4. A. DLOUHY, G. EGGELER and N. MERK, *Acta Metall. Mater.* **43** (1995) 535.
5. S. KÚDELA, V. GERGELY, A. SCHWEIGHOFER, S. BAUNACK, S. OSWALD and K. WETZIG, *J. Mater. Sci.* **29** (1994) 5071.
6. S. KÚDELA, V. GERGELY, L. SMRCOK, S. BAUNACK, S. OSWALD and K. WETZIG, *ibid.*, **31** (1996) 1597.
7. F. DEGRÉVE, N. A. THORNE and J. M. LANG, *ibid.* **23** (1988) 4181.
8. L. E. DAVIS, N. C. MAC DONALD, P. W. PALMBERG, G. E. RIACH and R. E. WEBER, "Handbook of Auger Electron Spectroscopy", 2nd Edn (Physical Electronics Industries, Eden Prairie, 1976).
9. G. HANKE and K. MÜLLER, *Surface Sci.* **152/153** (1985) 902.
10. T. W. CLYNE, M. G. BADER, G. R. CAPPLEMAN and P. A. HUBERT, *J. Mater. Sci.* **20** (1985) 85.
11. G. R. CAPPLEMAN, J. F. WATTS and T. W. CLYNE, *ibid.* **20** (1985) 2159.
12. S. KÚDELA, R. RENNEKAMP, S. BAUNACK, V. GERGELY, S. OSWALD and K. WETZIG, *Mikrochimica Acta* (to be published).
13. I. M. LOW and R. McPHERSON, *J. Mater. Sci.* **24** (1989) 926.
14. A. K. CHAKRAVORTY, *ibid.* **28** (1993) 3839.
15. "JANAF Thermochemical Tables", Vol. 37, 2nd Edn (US Department of Commerce NSRD-NBS, Washington, D.C., 1971) p. 1141.
16. Y. REPELIN and E. HUSSON, *Mater. Res. Bull.* **25** (1990) 611.
17. R. M. LEVY and D. J. BAUER, *J. Catal.* **9** (1967) 76.
18. B. HALLSTEDT, Z.-K. LIU and J. ÅGREN, *Mater. Sci. Eng.* **A169** (1993) 149.
19. L. A. PETROVA (ed.), "Constitution Diagrams of Metallic Systems" Vol. XXXIV (Vinti, Moscow, 1990) in Russian.
20. A. G. EVANS and B. J. DALGLEISH, *Mater. Sci. Eng.* **A162** (1993) 1.

*Received 22 June 1995*
*and accepted 3 October 1996*